Tendon Arrangement and Muscle Force Requirements for Humanlike Force Capabilities in a Robotic Finger

Nancy S. Pollard and Richards C. Gilbert

Brown University*

Abstract

Human motion can provide a rich source of examples for use in robot grasping and manipulation. Adapting human examples to a robot manipulator is a difficult problem, however, in part due to differences between human and robot hands. Even hands that are anthropomorphic in external design may differ dramatically from the human hand in ability to grasp and manipulate objects due to internal design differences. For example, force transmission mechanisms in robot fingers are generally symmetric about flexion / extension axes, but in human fingers they are focused toward flexion. This paper describes how a tendon driven robot finger can be optimized for force transmission capability equivalent to the human index finger. We show that two distinct tendon arrangements that are similar to those that have been used in robot hands can achieve the same range of forces as the human finger with minimal additional cost in total muscle force requirements.

1 Introduction

Teaching a robot by demonstration requires establishing the important features of a task [8], for example task impedance [3] or observable behavior of a controlled object [4]. Alternatively, tasks may be represented symbolically as a sequence of actions and desired state changes in the environment [17] [14].

While it will always be necessary to understand something about the task in order to execute it properly, duplicating an action from demonstration may be more straightforward when the static and dynamic characteristics of the robot are similar to those of the person demonstrating the action. Articulated robot hands often cite the human hand as design inspiration, and robot hands often have a design that is externally similar to the human hand. Even subtle functional capabilities are sometimes introduced. For example, Lovchik and Diftler [20] describe how the last two fingers of NASA's Robonaut Hand are mounted at an angle so that tools such as screwdrivers can be grasped in better alignment with the forearm and thus the roll axis of the wrist.

Internally, however, design of robot hands may differ greatly from that of the human hand. As one example, robot fingers can often apply identical forces in the directions of flexion and extension, but the human hand has strong asymmetry in these directions: flexion forces – the forces needed to form a power grasp of an object – have a much greater range than the forces that can be applied to extend the fingers.

[1]Contact: nsp@cs.brown.edu

In this paper, we compare force capabilities of the human index finger to those of two tendon-driven robot finger designs. We explore how these designs can be adapted to give the robot finger capabilities very similar to those of the human finger. For any choice of actuator, it is important to ensure adequate force capability. For some design choices, minimizing force that must be delivered to the tendons may lead to compactness in the resulting mechanisms. For McKibben-style pneumatic muscles [24], for example, cross-sectional area increases in proportion to maximum force. Minimizing force (and thus cross-sectional area) makes it more likely that these muscles could be used in a practical hand design [18] [12]. We show that tendon arrangements that are similar to those that have been used in robot hands [23] [13] can be tuned to achieve equivalent force capability with a cost – measured as the sum of maximum muscle forces – that is nearly identical to that of the human finger.

2 Background

For modeling the human finger, Valero-Cuevas [25] has shown that a linear model mapping muscle activation levels to contact forces is plausible for predicting forces that can be exerted by human subjects. Computing an achievable range of applied forces using such a model requires knowledge of link lengths, moment arms of tendons about the joints, and maximum muscle forces, all of which are available from [2] and [1].

McKibben-style actuators are of particular interest. Tondu and Lopez [24] give an overview of McKibben-style actuators. A number of robot hands have been developed with this type of actuator, including those of Caldwell et al. [7], Lee and Shimoyama [18], and the Shadow Robot Company [11]. Lee and Shimoyama point out the need to keep the cross-sectional area of these actuators small for use in hands, and they have developed a tendon-driven hand with extremely small muscles. The force capabilities of this hand, however, are almost an order of magnitude less than those of the human hand.

Many other types of robot hands have been developed (see [9] for an overview), and their force and passive compliance capabilities vary widely. This paper describes how any proposed design with anthropomorphic physical dimensions can be compared to the human hand in terms of force capability.

The ability to understand and control forces applied to an

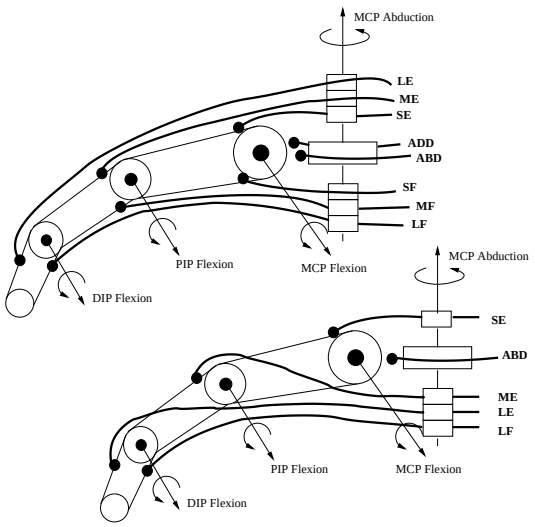

Figure 1: 2N and N+1 tendon robot fingers. N is the number of degrees of freedom of the finger (4 in this paper).

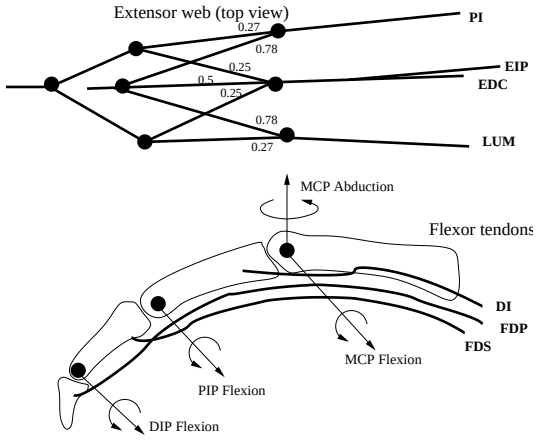

Figure 2: Flexor and extensor tendons of the human index finger. Numbers in the top figure indicate ratios of outgoing forces at each branch point in the extensor web.

object is critical for grasping and manipulation [23] [15]. Bicchi [6] gives an excellent survey of grasping and manipulation research and in [5] describes the contribution of hand kinematics to the force closure properties of a grasp. Force-based quality measures have been developed (e.g. [19] [16] [10] [22]), but these measures all work with an abstract contact model that does not take hand kinematics or force transmission mechanisms into account. More comprehensive force models such as that described here may help us better understand grasp quality and coordinated manipulation strategies.

3 Overview

This paper asks:

> Can the two tendon-driven finger designs in Figure 1 be tuned to have force capabilities equivalent to that of the human finger (Figure 2)?
>
> If so, do they represent higher or lower "cost" designs than that of the human finger? Cost is formalized as the sum over all tendons of the maximum force that must be supplied to that tendon.

Two tendon arrangements are explored: one that can be considered maximal: a $2N$ design with two tendons per degree of freedom, similar to that of the Utah/MIT hand [13], and one that can be considered minimal, an $N + 1$ design with one more tendon than degree of freedom, similar to the Stanford/JPL hand [23]. In this case, N is four; the finger is assumed to have four degrees of freedom: abduction / adduction at the MCP joint and flexion / extension at the MCP, PIP, and DIP joints.

To address the two questions above, we formalize equivalent force capability by requiring the space of all forces that can be applied by the robot finger to contain the space of forces that can be applied by the human finger. A single actuator or "muscle" is assumed to be attached to each tendon. The cost function (the sum of maximum forces that must be supplied to the tendons) is then mechanically justified by the desire to keep muscle size (and thus hand size) small.

The result is an optimization problem: find the lowest cost assignment of maximum forces to tendons that achieves force capability equivalent to that of the human finger. For the two designs in Figure 1, the global optimum can be found analytically when the fingers have the same link lengths and joint axis configurations as the human finger. Moment arms, or radii of the tendon pulleys in Figure 1, are a free design parameter and are numerically optimized.

Section 7 gives results of the optimization and our answers to the questions above:

> Muscle forces for both fingers in Figure 1 can be tuned so that they have force capabilities equivalent to that of the human finger.
>
> The cost is nearly identical to that of the human finger.

For a preview, see Figures 4 and 5 (for force capability, untuned vs. tuned) and Figure 6 (for cost).

4 Force Capabilities

For any given set of contact points, forces at the contacts are a linear function of forces supplied by the muscles to the tendons. Tendons create torques at all joint axes they cross, proportional to the moment arms of the tendons about the joint axes. In the bottom diagram of Figure 2, for example, force applied through the flexor digitorum profundus (FDP)

creates flexion torques at the DIP, PIP, and MCP joints and a small abduction torque at the MCP joint. Torques from all tendons are summed and mapped to forces at the contacts based on the kinematics of the device, the current pose, and the placement of the contact points.

Following the biomechanical literature, we assign each muscle an activation level from 0 (inactive) to 1 (at its maximum force). The mapping from activation levels to contact forces is then:

$$f = J^{+T} M P a \tag{1}$$

where a is the nx1 vector of muscle activation levels, with n the number of muscles (equal to the number of tendons). P converts activation levels to tendon forces and is $diag(p_1, ..., p_n)$, where p_i is the maximum muscle force that can be supplied to tendon i. M converts tendon forces to joint torques and contains joint moment arm information. J^{+T} is the pseudoinverse of the contact Jacobian, where J^T maps contact forces to joint torques and is dependent on finger pose. The Appendix contains details on how J, M, and P are obtained for the human and robot finger models as well as validation of the finger model using experimental human force measurements available in the literature.

Force capabilities are measured as the entire space of contact forces that can be achieved by the finger. For a given finger pose and a given choice of contact placement, this space of forces is contained within the convex hull of extreme forces f_k:

$$f_k = J^{+T} M P a_k, \quad k = 1, ..., 2^n \tag{2}$$

where a_k are corners of the n-dimensional unit activation hypercube, or the set of all combinations of minimally and maximally activated muscles. Extreme points in the space of applied forces are created by limits in activation levels – some tendons will be at their maximum force and some will be inactive. For a more complete description of this mapping from activation level space to force space, see [25].

5 Minimizing Muscle Size

We assume there is a cost to overdesigning a finger mechanism and use McKibben-style muscles as an example. McKibben-style muscles should ideally be small in diameter [18] [12] to keep hand size small. In these muscles, cross-sectional area is roughly proportional to force, and so we wish to minimize the sum of maximum muscle forces:

$$minimize \quad \sum_{i=1}^{muscles_R} p_{R,i} \tag{3}$$

where subscript R denotes a quantity of the robot finger, and $p_{R,i}$ is the maximum force required of muscle i for the robot finger.

Acceptable solutions are those where the force capabilities of the robot hand meet or exceed those of the human hand. More formally, for any pose and set of contact points, *the convex hull of $f_{R,k}$ must contain the convex hull of $f_{H,k}$* where:

$$f_{R,k} = J_R^{+T} M_R P_R a_{R,k}, \quad k = 1, ..., 2^{muscles_R} \tag{4}$$
$$f_{H,k} = J_H^{+T} M_H P_H a_{H,k}, \quad k = 1, ..., 2^{muscles_H} \tag{5}$$

Equations 4 and 5 are versions of Equation 2 with parameters specific to the robot and human hands under consideration. This form of the problem, however, is difficult to work with due to the dependence of the convex hulls of $f_{R,k}$ and $f_{H,k}$ on pose and contact point selection.

To simplify the problem of finding an acceptable solution, we observe that when the kinematic parameters of the two hands are identical, contact Jacobians J_R and J_H are identical, and it is sufficient to say that the torque capabilities of the robot hand must meet or exceed those of the human hand, or *the convex hull of $\tau_{R,k}$ must contain the convex hull of $\tau_{H,k}$*, where:

$$\tau_{R,k} = M_R P_R a_{R,k}, \quad k = 1, ..., 2^{muscles_R} \tag{6}$$
$$\tau_{H,k} = M_H P_H a_{H,k}, \quad k = 1, ..., 2^{muscles_H} \tag{7}$$

The convex hulls of $\tau_{R,k}$ and $\tau_{H,k}$ are independent of pose; comparing torque spaces is much easier than comparing force spaces.

We note that finding $\tau_{H,k}$ is trivial, because all parameters are known (see Appendix). The remaining problem is to find optimal maximum tendon forces $p_{R,i}$ along the diagonal of matrix P_R to satisfy the condition that the convex hull of $\tau_{R,k}$ must contain the convex hull of $\tau_{H,k}$. Two cases are discussed below: one where the mapping of joint torques to tendon forces is unique for a finger design and one where it is not.

5.1 Case 1: Unique Torque to Force Mapping

For the finger designs in Figure 1, finding globally optimal muscle force assignments $p_{R,i}$ is straightforward. A simple solution is possible because the muscle forces required to achieve any given torque are unique if co-contractions producing no net torque are ignored. For example, finger forces required to achieve a given torque $\tau_{H,k}$ for the $2N$ design can be found by construction by working inward from the DIP joint:

$$p_{R,LF,k} = \left\{ \begin{array}{ll} \frac{\tau_{H,k,DIP}}{M_{R,DIP,LF}} & \tau_{H,k,DIP} > 0 \\ 0 & \tau_{H,k,DIP} \leq 0 \end{array} \right\}$$

$$p_{R,LE,k} = \left\{ \begin{array}{ll} 0 & \tau_{H,k,DIP} > 0 \\ \frac{\tau_{H,k,DIP}}{M_{R,DIP,LE}} & \tau_{H,k,DIP} \leq 0 \end{array} \right\}$$

$$\tau'_{H,k,PIP} = \tau_{H,k,PIP} - p_{R,LF,k} M_{R,PIP,LF} + p_{R,LE,k} M_{R,PIP,LE}$$

$$p_{R,MF,k} = \left\{ \begin{array}{ll} \frac{\tau'_{H,k,PIP}}{M_{R,PIP,MF}} & \tau'_{H,k,PIP} > 0 \\ 0 & \tau'_{H,k,PIP} \leq 0 \end{array} \right\}$$

$$p_{R,ME,k} = \left\{ \begin{array}{cc} 0 & \tau'_{H,k,PIP} > 0 \\ \frac{\tau'_{H,k,PIP}}{M_{R,PIP,ME}} & \tau'_{H,k,PIP} \leq 0 \end{array} \right\}$$

Remaining forces $p_{R,i,k}$ for the $2N$ design and forces for the $N+1$ design are found in a similar manner.

This unique torque to force mapping means that there is really no optimization to be done: the maximum force required for any tendon is the worst case force for that tendon over all torques $\tau_{H,k}$ on the convex hull of the human finger torque space. For tendon LF for example:

$$p_{R,LF} = \max_{k=1}^{2^{muscles_H}} (p_{R,LF,k}) \quad (8)$$

In other words, the maximum required force $p_{R,i}$ for tendon i is the maximum force required to support the worst case torque $\tau_{H,k}$ for that tendon.

5.2 Case 2: Non-Unique Torque to Force Mapping

For some finger designs, a global optimum cannot be found in this manner. If there is not a unique set of muscle forces that will achieve a given torque, then it is not obvious what is the best $p_{R,i,k}$ corresponding to a given torque $\tau_{H,k}$. For example, if an MF tendon is added to the $N+1$ design, it is not clear how much force to assign to MF and how much to assign to co-contraction of LE and LF. Assigning the force to MF may make MF needlessly large if co-contraction forces for LE and LF will be available due to the requirements of achieving $\tau_{H,k}$ for other values of k.

Although it does not in general produce a global minimum, the following approach can be used to find a good initial guess. The force needed to achieve a given torque $\tau_{H,k}$ is formulated as a linear programming problem.

$$minimize \quad \sum_{i=1}^{muscles_R} p_{R,i,k} \quad (9)$$

Subject to:

$$M_R p_{R,k} = \tau_{H,k} \quad (10)$$

$$p_{R,i,k} \geq 0, \quad i = 1, ..., muscles_R \quad (11)$$

Equation 8 is employed as before:

$$p_{R,i} = \max_{k=1}^{2^{muscles_H}} (p_{R,i,k}), \quad i = 1, ...muscles_R \quad (12)$$

with $p_{R,i,k}$ obtained by solving the problem in Equations 9 through 11 for each k. This initial set of muscle forces is then sent to a numerical optimization routine to minimize the overall objective function in Equation 3.

This approach was tested on the human finger design, where a given torque can in general be achieved with an open-ended space of tendon force combinations. The initial guess of Equation 12 returned the actual forces used for the human finger model with one exception: the lumbrical force was computed to be $89.5N$ instead of the required $12.6N$. Numerical optimization quickly reduced lumbrical force to $12.6N$ and terminated with the original set of human finger maximum forces.

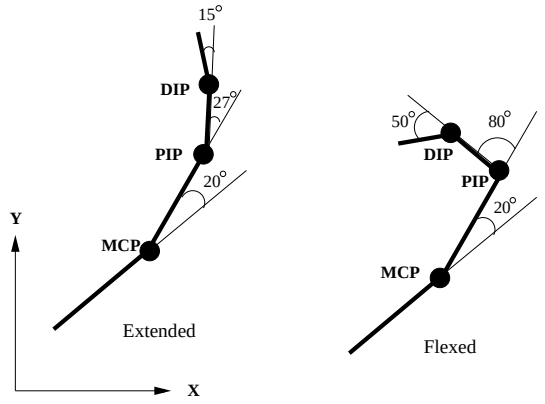

Figure 3: The two poses selected for graphical display of fingertip force capabilities in Figures 4 and 5.

6 Optimizing Moment Arms

One set of free design parameters for the robot finger is the moment arms at the joints. Moment arms do affect force requirements. For example, if the moment arms for flexors and extensors about the MCP abduction / adduction joint are large, then large forces in the ABD and ADD muscles will be required to counteract these forces when pure flexion or extension is desired.

To investigate whether the moment arms could be improved, we divided them into five groups and invoked a numerical optimizer (Powell's direction set algorithm) to minimize total cross-sectional area. The five groups were: DIP flexion / extension, PIP flexion / extension, MCP flexion / extension, MCP abduction / adduction by ABD and ADD, and MCP abduction / adduction by all other tendons. In each iteration of the optimization, tendon forces were computed as described in Section 5.1. Moment arms were limited to those seen in the human finger (Figure 7), both to allow for a more fair comparison of cross-sectional areas and to respect plausible mechanical limits. These limits were "soft:" the objective function included a penalty proportional to distance beyond the limits.

In the case where the torque to force mapping is not unique (Section 5.2), moment arms can be added as additional parameters in the final search for optimal forces. In practice this approach has also worked well; the search landscape does not appear to be complex in the moment arm directions.

7 Results

Figure 4 displays the space of forces that can be applied at the fingertip for the human finger and an untuned $2N$ robot

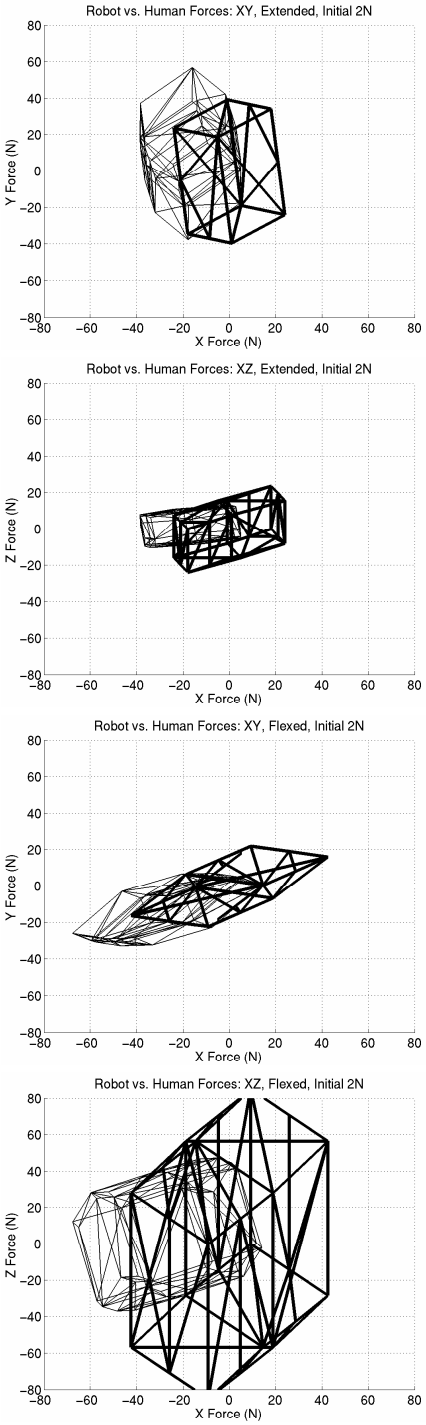

Figure 4: Force capabilities for the human and initial $2N$ robot finger. Results from the extended (top) and flexed (bottom) pose are shown in two views each (XY and XZ). Thin lines denote the human finger and thick lines denote the robot finger. For reference, the geometry of the two poses is rendered in the XY plane in Figure 3.

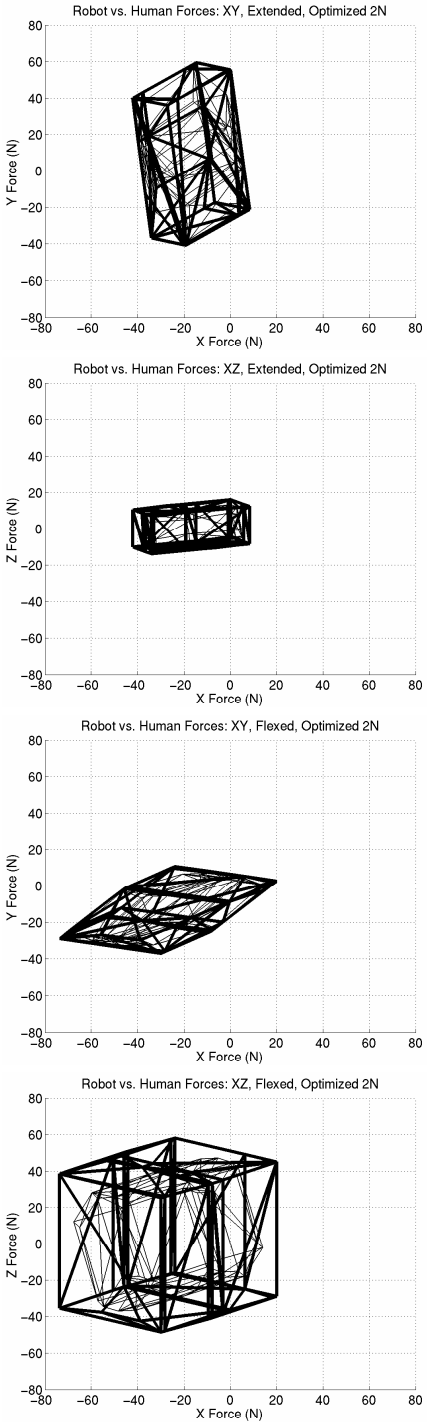

Figure 5: Force capabilities for the human and optimized $2N$ robot finger. Results from the extended (top) and flexed (bottom) pose are shown in two views each (XY and XZ). Thin lines denote the human finger and thick lines denote the robot finger. The force space for the human finger is the same as in Figure 4.

Tendon	Initial $2N$	Optimized $2N$	Initial $N+1$	Optimized $N+1$
LE	71.7N	28.2N	114.8N	79.8N
LF	71.7N	141.4N	114.8N	209.3N
ME	71.7N	8.8N	114.8N	65.2N
MF	71.7N	104.7N	N/A	N/A
SE	71.7N	59.1N	114.8N	118.5N
SF	71.7N	130.3N	N/A	N/A
ABD	71.7N	79.1N	114.8N	101.3N
ADD	71.7N	46.1N	N/A	N/A
Total	574N	598N	574N	574N
% Human	100%	104%	100%	100%

Figure 6: Muscle forces for the initial and optimized designs of each robot finger. The initial designs are far from duplicating the force capabilities of the human finger model (Figure 4), while the optimized designs can duplicate these force capabilities (Figure 5).

finger design. (See Appendix for design details.) Two poses are shown (Figure 3) and two views are shown of each pose. Contact conditions such as contact normal and friction cone are ignored to illustrate the full set of forces that could be applied at the fingertip based on the mechanics of the device. A particular choice of contact normal and surface properties would constrain the valid set of forces to a subset of this space. Note especially the symmetry about the origin of the force space of the robot finger (thick lines) compared to the very strong asymmetry of the human finger (thin lines).

Figure 5 shows the same set of plots after maximum forces and moment arms of the $2N$ robot finger have been optimized. The set of forces the robot finger can exert at the fingertip now contains the set of forces the human finger can exert at the fingertip. Although a single contact point (the fingertip) was selected for illustration, similar results hold for any contact point or collection of contact points on the finger due to the guarantee that the convex hull of $\tau_{R,k}$ contains the convex hull of $\tau_{H,k}$ (Section 5).

Figure 6 compares the muscle forces and sum of force values for the initial and optimal designs. Total cost for both designs (measured as the sum of maximum forces) is very similar to that of the human finger. Optimized moment arms are shown in Figure 7. Figures 6 and 7 also show data for the $N+1$ design. Force space plots for the $N+1$ design were not included for space reasons, but are identical in character to those in Figures 4 and 5.

8 Discussion

Muscle forces and moment arms of two tendon driven robot finger designs were optimized to duplicate the force capabilities of the human finger with very similar total muscle force requirements. The good match of both force capability (Figure 5) and cost (sum of muscle forces in Figure 6) is somewhat surprising given that the robot finger designs differ from the human finger and from each other in number of tendons, roles of each tendon, and tendon moment arms,

Moment Arm Group	Limit (mm)	$2N$ Optimized Result (mm)	$N+1$ Optimized Result (mm)
Flex/Ext Abd/Add	12.0	1.4	2.0
Abd/Add	12.0	12.0	12.0
MCP Flex/Ext	12.0	12.0	12.0
PIP Flex/Ext	8.0	8.0	8.0
DIP Flex/Ext	4.0	4.2	4.1

Figure 7: Robot finger moment arms: (soft) limits derived from the human finger and results found by the optimization process. The Flex/Ext Abd/Add group is the moment arm created about the MCP abduction / adduction degree of freedom by any flexor or extensor. The Abd/Add group is the moment arm created about the same axis by the ABD or ADD tendon. The other three groups represent moment arms about the three flexion / extension degrees of freedom.

with the robot fingers designed for simpler manufacture. If McKibben-style muscles are used to construct such a finger, focusing force requirements can keep cross-sectional area of muscles to a minimum, helping to keep hand size small.

It is interesting to note that we were able to use this optimization approach to select the best $N+1$ tendon design – that shown in Figure 1. There are eight plausible tendon arrangements for the $N+1$ design: the long tendons can either flex or extend the PIP joint, the long and medium tendons can either flex or extend the MCP joint, and the long, medium, and short tendons can either abduct or adduct the MCP joint. The design shown in Figure 1 was selected because it was the best of the eight tendon arrangements, with the lowest required sum of maximum tendon forces. For comparison, the cost of the selected design was 574N. The costs of the other seven designs ranged from approximately 640N (when abduction / adduction roles were switched) to 1380N (when *all* tendon roles were switched – i.e. the inverse of the design in Figure 1).

There are some differences between the $2N$ and $N+1$ designs. First, stiffness control will differ. For either design, it may be possible to increase stiffness by co-contraction, but the $N+1$ design dramatically magnifies co-contraction forces distal to proximal. Second, the $N+1$ design mixes extension and flexion roles within the same tendons. Tendons that are extensors at their distal attachments are flexors at more proximal joints. This condition is also partially true of the human finger. The lateral bands of the human finger extensor mechanism are MCP flexors (Figure 9, PI and LUM).

Different arrangements of tendons or additional tendons would make either system more redundant. A number of alternative designs were evaluated using the technique for redundant combinations of tendons described in Section 5.2. For the purposes of matching human finger force capabilities, none were superior to those in Figure 1. Such designs are potentially interesting, however, because like the human finger, they provide some level of robustness to failure: if one of the tendons fails, the finger may still preserve much of its function. Finding good measures for robustness that would

Link			Length (cm)
MCP Abd	→	MCP Flex	0
MCP Flex	→	PIP	4.70
PIP	→	DIP	2.57
DIP	→	tip	2.24

Figure 8: Link lengths used for both human and robot models. Lengths are measured between joint positions and to the tip of the bony part of the finger.

allow a more fair evaluation of these alternative designs is a problem that deserves further investigation.

Range of motion must also be considered in any practical design. Some of the tendons may have a range of motion of approximately 4cm, and good force control would be needed over this range.

Design of the MCP joint must also be adjusted for practicality. This paper assumes that MCP flexion / extension is co-located with MCP abduction / adduction. Offsetting the MCP abduction / adduction axis as in the Utah/MIT hand design [13], for example, would require increasing maximum force requirements of some or all of the tendons.

Our long-term hypothesis is that a significant fraction of successful grasping behavior derives from the mechanical design of the hand. We have shown that human force capability can be matched in a robot hand design. Matching this and other properties such as stiffness may make it easier for us to successfully imitate human grasps. Testing this hypothesis is a topic of future work.

Acknowledgments

We would like to thank Jessica Hodgins, Jehee Lee, and Chris Atkeson for their helpful comments on drafts of this paper. This work was supported by NSF grant CCR-0093072.

Appendix: Finger Models

Human Finger Model

Following Valero-Cuevas et al. [25], the human index finger is modeled as shown in Figure 2. The finger is assumed to have four degrees-of-freedom, with rotational axes as shown in the figure. There are three degrees-of-freedom for flexion / extension at distal interphalangeal (DIP) joint, the proximal interphalangeal (PIP) joint, and the metacarpophalangeal (MCP) joint. There is one degree-of-freedom for abduction / adduction at the MCP joint.

Link lengths, moment arms, and maximum force per tendon are tabulated in Figures 8, 9, and 10. Link lengths and moment arms were obtained from [2] and are an average over seven hand specimens. Moment arms are also an average over the range of motion of each joint.

Tendon	MCP Abd	MCP Flex	PIP Flex	DIP Flex
FDP	-1.1	11.1	7.9	4.1
FDS	-1.7	11.9	6.2	-
DI	6.1	3.7	-	-
EDC	0.2	-8.6	-2.6	-1.9
EIP	-1.3	-9.0	-2.6	-1.9
PI	-5.8	6.6	-2.6	-1.9
LUM	4.8	9.3	-2.6	-1.9

Figure 9: Moment arms (mm) for each tendon of the human finger model about each degree-of-freedom.

Tendon	Max Force (N)
flexor digitorum profundus (FDP)	143.5
flexor digitorum superficialis (FDS)	127.8
first dorsal interosseous (DI)	145.6
extensor digitorum communis (EDC)	48.7
extensor indicis proprius (EIP)	39.2
first palmar interosseous (PI)	56.0
first lumbrical (LUM)	12.6

Figure 10: Maximum forces for each tendon of the human finger model.

Following [25] maximum muscle force is obtained for each tendon using physiological cross-sectional area (PCSA) numbers from [1] and a conversion from PCSA to force of $35N/cm^2$. In the human finger extensor mechanism, the tendons split and merge. An estimate of force distribution at each split is shown in Figure 2 and is obtained from [25].

The human finger force model was compared to experimental results published in the literature, specifically Milner and Franklin [21]. Two poses were tested (Figure 3). The coordinate system and flexion joint angles are shown in the figure. The MCP abduction angle is zero for both poses.

Figure 11 compares the maximum fingertip forces obtained by our model to the experimental results in [21]. The experimental data show the average and standard deviation for five male subjects between the ages of 23 and 29 who were asked to apply maximum fingertip forces in specific directions. The modeled results show the same general trends as the experimental data, with the exception of forces in the negative y direction for the flexed pose. This particular data point has the highest standard deviation of all the measurements, and our model results also show high variability with force direction, link length, and pose due to sensitivity of the moment arm about the MCP joint to these parameters (Figure 3). We found the overall agreement of model and experiment to be encouraging, especially given the fact that the data for the finger model was derived from a different set of subjects than those who participated in the experiments. It should eventually be possible to develop more accurate models for individual subjects by taking advantage of improvements in MRI speed, resolution, and data processing to extract actual link lengths, joint positions, and moment arms

Pose	Src	x	-x	y	-y
Ext	Exp	10.6 [1.5]	49.7 [4.9]	31.0 [5.6]	26.9 [7.4]
Ext	Mod	4.3	36.8	27.7	20.2
Flx	Exp	11.2 [1.8]	45.2 [9.5]	10.9 [2.5]	49.6 [19.4]
Flx	Mod	12.8	30.0	5.8	12.6

Figure 11: Comparison of human index finger model maximum forces to maximum forces measured from human subjects. Two poses were tested, an extended (Ext) and a flexed (Flx) pose. The source is either the human model (Mod) or the experimental data (Exp). Experimental data is taken from [21] and the standard deviation is given in square brackets.

Tendon	MCP Abd		MCP Flex		PIP Flex		DIP Flex	
	2N	N+1	2N	N+1	2N	N+1	2N	N+1
LE	4	-3	-12	12	-8	8	-4	-4
LF	-4	-3	12	12	8	8	4	4
ME	4	-3	-12	12	-8	-8	-	-
MF	-4	N/A	12	N/A	8	N/A	-	N/A
SE	-4	-3	-12	-12	-	-	-	-
SF	4	N/A	12	N/A	-	N/A	-	N/A
ABD	12	12	-	N/A	-	N/A	-	N/A
ADD	-12	N/A	-	-	-	-	-	-

Figure 12: Moment arms (mm) for each tendon of the robot finger model about each degree-of-freedom. Both the 2N and the N+1 configurations are shown.

as functions of finger configuration.

Robot Finger Models

The robot finger models are a $2N$ and an $N + 1$ tendon-driven design, shown in Figure 1. In the Figure, the MCP Abduction axes are drawn separate from the MCP Flexion axes for clarity, but in the models, the link parameters are the same as those for the human finger (Figure 8) and these axes are co-located.

For the $2N$ design, there are two tendons for each degree-of-freedom, and the tendons assigned to the more distal degrees-of-freedom also cross the more proximal joints. The design is similar to that of the Utah-MIT hand [13], although link lengths have been scaled to the human finger model. Moment arms are initially set to values given in Figure 12. Tendon forces are initially set to $71.7N$ for each tendon to match the sum of forces available in the human hand model. This number is similar to the very conservative estimate of $90N$ given in [13] for the actual hand.

For the $N+1$ design, there is one more tendon than degree of freedom. This is a minimal design, and is similar to that of the Stanford-JPL hand [23], although the Stanford-JPL hand had three degrees of freedom per finger instead of four. Moment arms are initially set as shown in Figure 12, and tendon forces are set to $114.8N$ for each tendon to match the sum of forces available in the human hand model.

References

[1] K. An, E. Chao, W. Cooney, and R. Linscheid. Forces in the normal and abnormal hand. *Journal of Orthopaedic Research*, 3:202–211, 1985.

[2] K. N. An, Y. Ueba, E. Y. Chao, W. P. Cooney, and R. L. Linscheid. Tendon excursion and moment arm of index finger muscles. *Journal of Biomechanics*, 16:419–425, 1983.

[3] H. Asada and Y. Asari. The direct teaching of tool manipulation skills via the impedance identification of human motion. In *Proc. IEEE Intl. Conference on Robotics and Automation*, 1988.

[4] C. G. Atkeson and S. Schaal. Robot learning from demonstration. In *International Conference on Machine Learning*, 1997.

[5] A. Bicchi. On the closure properties of robotic grasping. *International Journal of Robotics Research*, 14(4):319–334, 1995.

[6] A. Bicchi. Hands for dexterous manipulation and robust grasping: A difficult road toward simplicity. *IEEE Transactions on Robotics and Automation*, 16(6):652–662, 2000.

[7] D. G. Caldwell, G. A. Medrano-Cerda, and M. J. Goodwin. Braided pneumatic actuator control of a multi-jointed manipulator. In *Proc. IEEE Intl. Conference on Systems, Man, and Cybernetics*, pages 423–428, 1993.

[8] R. Dillmann, H. Friedrich, M. Kaiser, and A. Ude. Integration of symbolic and subsymbolic learning to support robot programming by human demonstration. In G. Giralt and G. Hirzinger, editors, *Robotics Research: The Seventh International Symposium*. Springer, New York, 1996.

[9] C. Laschi et al. Grasping and manipulation in humanoid robotics. In *Proc. IEEE RAS Workshop on Humanoids*, 2000.

[10] C. Ferrari and J. Canny. Planning optimal grasps. In *Proc. IEEE ICRA*, Nice, France, May 1992.

[11] Dexterous Hand/Arm. *Shadow Robot Company*. http://www.shadow.org.uk/products/hand.shtml.

[12] B. Hannaford, J. M. Winters, C.-P. Chou, and P.-H. Marbot. The anthroform biorobotic arm: A system for the study of spinal circuits. *Annals of Biomedical Engineering*, 23:399–408, 1995.

[13] S. C. Jacobsen, J. E. Wood, D. F. Knutti, and K. B. Biggers. The UTAH/M.I.T. dextrous hand: Work in progress. *International Journal of Robotics Research*, 3(4):21–50, Winter 1984.

[14] S. B. Kang and K. Ikeuchi. Toward automatic robot instruction from perception – temporal segmentation of tasks from human hand motion. *IEEE Transactions on Robotics and Automation*, 11(5):670–681, 1995.

[15] J. Kerr and B. Roth. Analysis of multifingered hands. *International Journal of Robotics Research*, 4(4):3–17, 1986.

[16] D. G. Kirkpatrick, B. Mishra, and C. K. Yap. Quantitative Steinitz's theorems with applications to multifingered grasping. In *Proc. 20th ACM Symposium on Theory of Computing*, Baltimore, Maryland, May 1990.

[17] Y. Kuniyoshi, M. Inaba, and H. Inoue. Learning by watching: Extracting reusable task knowledge from visual observation of human performance. *IEEE Transactions on Robotics and Automation*, 10(6):799–822, 1994.

[18] Y. K. Lee and I. Shimoyama. A skeletal framework artificial hand. In *Proc. IEEE Intl. Conference on Robotics and Automation*, 1999.

[19] Z. Li and S. Sastry. Optimal grasping by multifingered robot hands. In *Proc. IEEE Intl. Conference on Robotics and Automation*, Raleigh, North Carolina, 1987.

[20] C. S. Lovchik and M. A. Diftler. The robonaut hand: A dexterous robot hand for space. In *Proc. IEEE Intl. Conference on Robotics and Automation*, 1999.

[21] T. E. Milner and D. W. Franklin. Characterization of multijoint finger stiffness: Dependence on finger posture and force direction. *Transactions on Biomedical Engineering*, 45(11):1363–1375, 1998.

[22] N. S. Pollard. Synthesizing grasps from generalized prototypes. In *Proc. IEEE Intl. Conference on Robotics and Automation*, Minneapolis, Minnesota, April 1996.

[23] J. K. Salisbury and J. J. Craig. Articulated hands: Force control and kinematic issues. *IJRR*, 1(1), Spring 1982.

[24] B. Tondu and P. Lopez. Modeling and control of mckibben artificial muscle robot actuators. *IEEE Control Systems Magazine*, 20(2):15–38, 2000.

[25] F. J. Valero-Cuevas, F. E. Zajac, and C. G. Burgar. Large index-fingertip forces are produced by subject-independent patterns of muscle excitation. *Journal of Biomechanics*, 31:693–703, 1998.